PROPAGATION MEASUREMENTS FOR THE AERONAUTICAL SATELLITE CHANNEL

Andreas Neul, Joachim Hagenauer, Wolfgang Papke, Frank Dolainsky
Franz Edbauer

German Aerospace Research Establishment (DFVLR)
Institute for Communication Technology
D-8031 Oberpfaffenhofen

ABSTRACT

Although there is a variety of system design proposals for aeronautical satellite communications, only a few field trials have been accomplished to investigate the behaviour of the aeronautical satellite transmission channel.
The German Aerospace Research Establishment (DFVLR) finished in May 86 an extensive test program to provide necessary information for a system design. Over one thousand minutes of useable test signals could be recorded. With these recordings a detailed statistical evaluation had been performed.

INTRODUCTION

In recent years a variety of proposals for an aeronautical satellite communications system at L-band frequencies came up. Although it is known that data transmission suffers from multipath effects caused by reflections from the earth's surface, only a few field trials have been accomplished to investigate the behaviour of the aeronautical surface scatter channel. In this paper, the results of a measurement campaign [1] are presented. In seventeen flights with a twin jet "FALCON" more than one thousand minutes of useable test signals could be recorded and were evaluated. To guarantee a maximum degree of stationarity, the flights were conducted along routes with constant elevation angle to the Atlantic-Ocean-Region MARECS satellite (Figure 1.1).

Section 2 summarizes the theoretical channel model as a basis for the channel probing principle. Measurement results concerning propagation parameters and fading statistics are presented in section 3. Bit-error rate curves obtained from inflight as well as stored channel measurements are given in section 4.

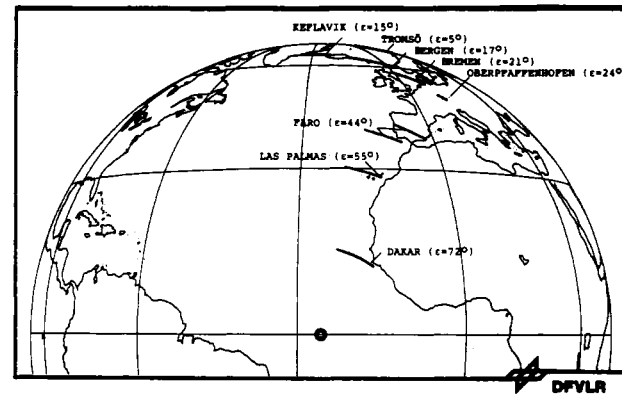

Fig. 1.1: Flightroutes from AOR-MARECS satellite view

PRINCIPLES OF CHANNEL EVALUATION TESTS

Theoretical Channel Model

The geometry of the communication channel "satellite-aircraft" is shown in Fig. 2.1.

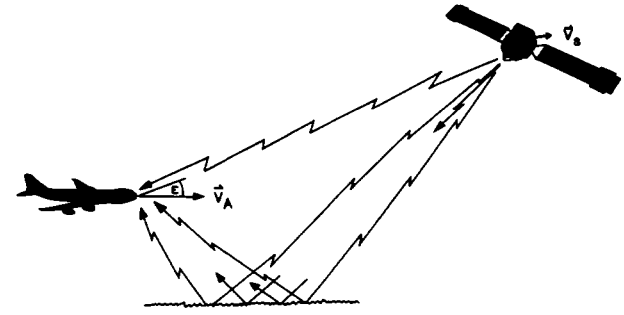

Fig. 2.1: Geometry "satellite-aircraft" communication channel

If the satellite transmits a signal x(t) then the aircraft receives in general two components. The direct component $y_d(t-t_o)$ and the reflected (multipath) component, from the earth

CH2429-9/87/0000-0090 $1.00

surface $y_r(t-t_o-\tau)$. The propagation delay t_o has no influence on the channel model and is therefore neglected in further considerations. The differential delay τ depends basically on the geometry. It can be calculated as a function of the elevation angle ε and is shown in Fig. 2.2 for different aircraft altitudes.

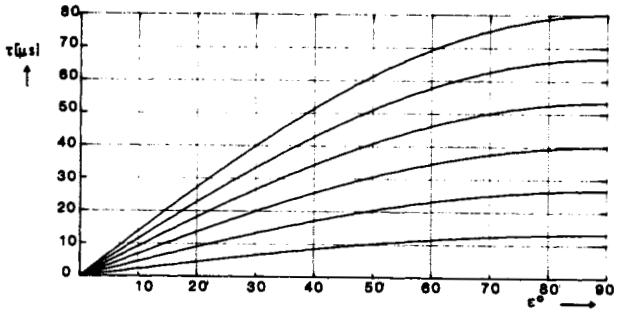

Fig. 2.2: Time differences between direct and reflected signal with altitude h as parameter. (from 2 km to 12 km)

The signal y(t) at the receiver of the aircraft results from the addition of the direct and the reflected component at the antenna used. This multipath reception is the reason for signal fading. As the reflection coefficient of land is much smaller than that of salt-water, the following considerations concentrate on multipath reception from the sea.

Due to aircraft motion and the roughness of the earth surface, the aeronautical channel in principle has to be modelled as a randomly time-variant channel. The theory of randomly time-variant linear channels is described in a fundamental paper by Bello [2]. Applying this to the aeronautical circumstances, the reflected signal component can be seen as transmitted over a wide-sense stationary uncorrelated scatterer (WSSUS) channel [3,4]. For all signal bandwidths B considered [5], this channel is described by multiplicative (non frequency selective) fading, i.e. the time variant transfer function T(f,t) is independent of frequency within these ranges:

$$T(f,t) = T(t) \text{ for } f_o - \frac{B}{2} < f < f_o + \frac{B}{2} \quad (1)$$

f_o = carrier frequency

Therefore, the aeronautical channel model shown in Fig. 2.3 can be assumed. I(t) and Q(t) are the inphase- and the quadrature phase component of T(t).

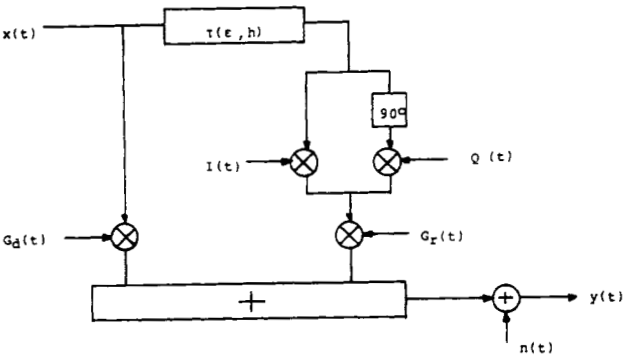

Fig. 2.3: Aeronautical channel model

The factors $G_d(t)$ and $G_r(t)$ represent the attenuation in direction to the direct and reflected path resulting from link conditions (free space loss, antenna gain etc.). In general, they are not constant because the motion of the aircraft changes the relative position to the satellite.

Channel Probing

The time-variant transfer function T(f,t) is just equal to the complex modulation observed on a received carrier transmitted at frequency f. Therefore, I(t) and Q(t) from Fig. 2.3 can be obtained by probing the reflected component of the aeronautical channel with a stable continuous wave (CW-)carrier transmitted from the satellite (Fig. 2.4).

The received signal at the aircraft is to be mixed down to baseband and the inphase and quadrature phase fading components I(t) and Q(t) are to be low-pass filtered for noise suppression. With I(t) and Q(t) all amplitude and phase variations caused by the transmission are known.

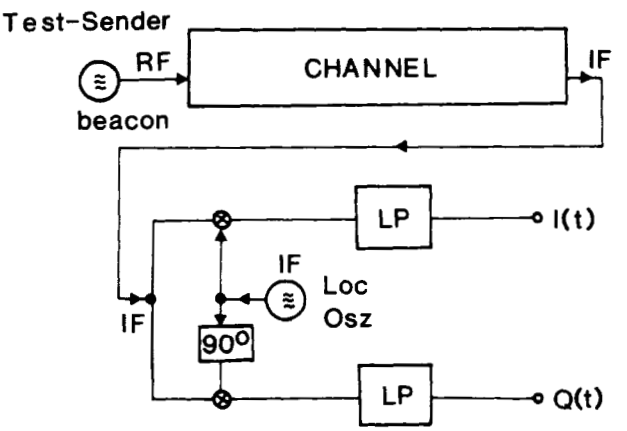

Fig. 2.4: Channel probing principle

When applying the channel prober principle to mobile satellite channels with low G/T values at the mobile termi-

nals, it is very important to receive the signals essentially noisefree. This means that the bandwidth of the filters in Fig. 2.4 has to be as small as possible.

On the other hand the doppler shift due to fading and aircraft motion should be accomodated. Doppler shifts due to aircraft motion in the direct (unfaded) signal were compensated by an AFC control loop in the receiver. The same frequency control voltage was used to control the frequency in the receiver path of the reflected (fading) signal. Taking this frequency control into account a filter bandwidth of 1 kHz for the reflected signal and of 200 Hz for the direct signal, was chosen.

To assure furthermore an appropriate dynamic range for fading measurement a satellite EIRP of 27 dBW (ten voice channels) was provided. So, the mean C/N_O was 53 dBHz and in the reflected signal fades down to 23 dB could be detected.

Measurement System

Four different antenna units were installed at the aircraft (Fig. 2.5):

- o a conformal, electronically steerable, phased array (10 dB gain) [6], mounted on the upper left side for reception of the direct signal.
- o a mechanically steerable helix antenna (10 dB) installed near the tail, pointing towards the specular reflection point; it has two radiators, one for reception of the right hand circular and one for LHC polarized waves.
- o a printed patch element (B-antenna, 5 dB) and
- o a crossed dipole (K-antenna,3 dB),

both fixed behind one of the windows as possible operational antennas for the reception of the combined direct plus reflected signal.

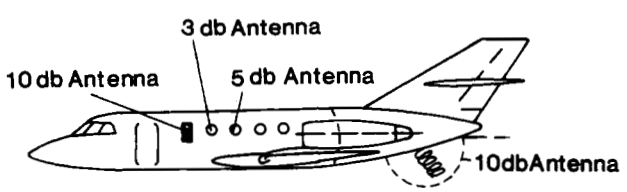

Fig. 2.5: Antenna positions at the aircraft

The direct and reflected signal had been received by two separate receiver chains [see Fig. 2.6], in which the L-band signal was downconverted to an IF-frequency of 70 MHz in the frontend, fed through an IF amplifier, mixed down to baseband in the channel prober, filtered and finally recorded on analog tape. These recordings of the direct and reflected signals can be used in the laboratory together with the stored channel simulator [7], to simulate all desired antenna patterns. Furthermore, a precise statistical offline evaluation can be performed.

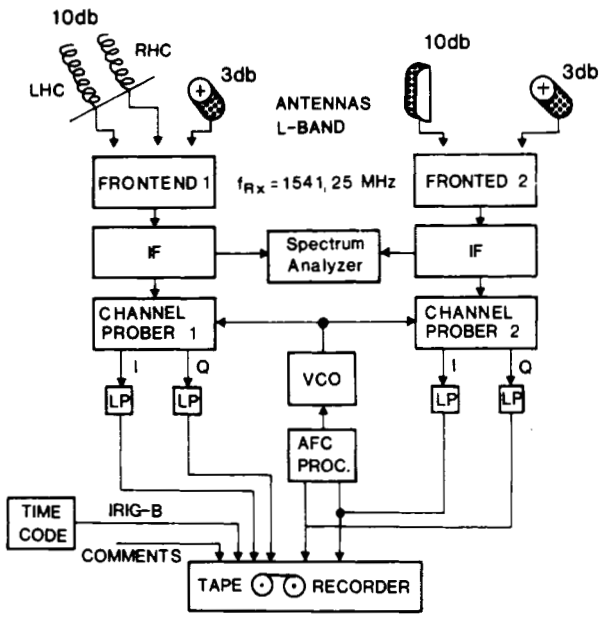

Fig. 2.6: Onboard measurement system

PROPAGATION MEASUREMENT RESULTS

Rice-factor C/M

The measured ratios "directly received power C" to "right-hand-circular multipath power M" for an ideal 0 dBi antenna is shown in Fig. 3.1 as a function of the elevation angle ε. In a wide range, there is a good coincidence to the C/M derived from Fresnel's reflection coefficients for specular reflections and the divergence factor [8].

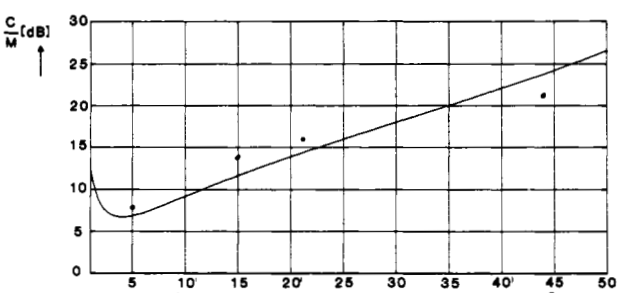

Fig. 3.1: C/M vs. elevation angle

Bandwidth of Doppler-Power-Spectra

For flights along routes with constant elevation angle, there is no deterministic Doppler component. Then, according to the theory in [3] the Doppler-power-spectrum of the reflected signal has a Gaussian shape

$$P(\nu) = \frac{\sqrt{2}}{B_{rms}\sqrt{\pi}} \exp\left(-\frac{2\nu^2}{B^2_{rms}}\right) \qquad (2)$$

This Gaussian shape was verified in all measurements (see for example Fig. 3.2).

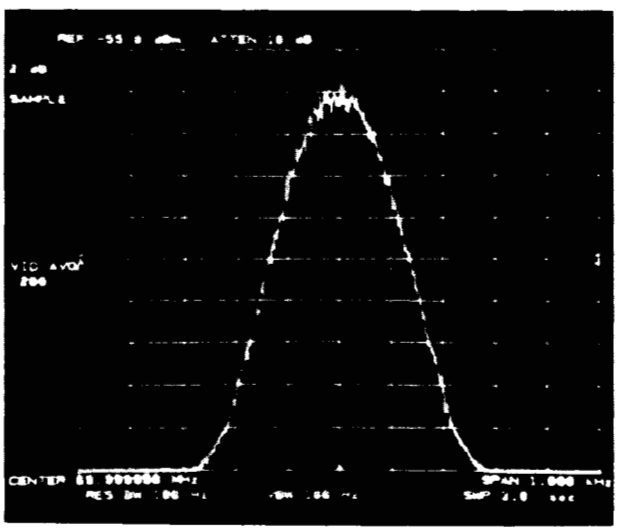

Fig. 3.2: Power-spectrum of RHC reflected signal at $\varepsilon = 15^o$ elevation angle

In (2) the rms Doppler spread is defined as twice the standard deviation of P(ν)

$$B_{rms} = 4\,\frac{\alpha}{\lambda_o} \cdot v \cdot \sin\varepsilon \qquad (3)$$

where α is the rms value of the surface slope, λ_o the wavelength of the transmitted carrier and v the speed of the aircraft along the route with constant elevation angle. Figure 3.3 shows measured values for B_{rms}, compared to the above equation with α equals to 0.04, 0.12 and 0.2, λ_o= 0.2 m and v=380 knots/h.

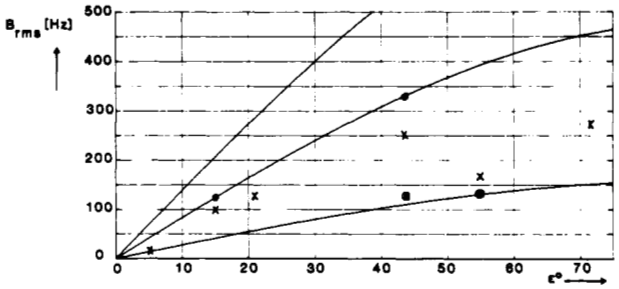

Fig. 3.3: Measured Doppler-Spread Values
x LHC at flight level 3000
O RHC at flight level 3000
⊠ LHC at flight level 600

Note that there is a tendency for decreasing Doppler-spread with decreasing altitude.

Evaluation of normalized Envelope Power

For a statistical offline investigation from all I(t) and Q(t) recordings the momentary normalized envelope power has been calculated by

$$P(t) = \frac{I(t)^2 + Q(t)^2}{\bar{P}} \qquad (4)$$

where $\bar{P}$ is the mean received power.

This data was then processed in further steps. In the following, some of the results are summarized.

Probability-Distribution-Function of Reflected Signal

In cases, where direct and received signal had been received separately, it was proved that the reflected signal always was exactly Rayleigh-distributed. Fig. 3.4 shows this as an example for the $\varepsilon = 15^o$ flight. In the Rayleigh paper used, the solid straight line represents the theoretical Rayleigh-distribution. Crosses are obtained from measured data.

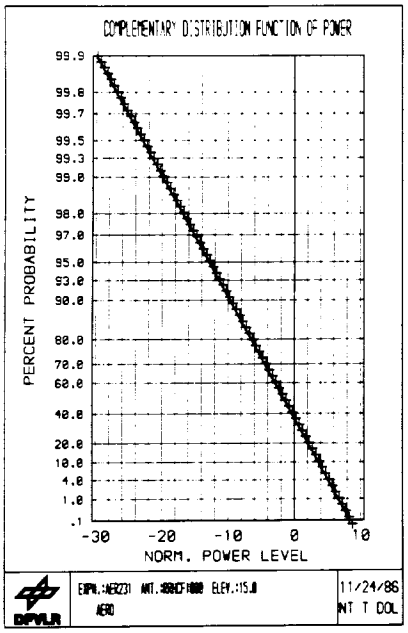

Fig. 3.4: Percentage of time that signal level is above normalized power level

Results for Preoperational 3 dB Antenna

It can be shown [1] that for signal bandwidth in the range of a few kHz, the delay τ can be neglected and the composite direct and reflected signal together can be modelled by multiplicative fading. The probability-distribution-function has then a Rician-shape; the Rice-factor C/M depends heavily on the effective antenna pattern. For the 3 dB antenna used in the measurements described above, the C/M values shown in Fig. 3.5 were extracted from a chi-square parameter fit of the experimental data to the theoretical Rician-curve.

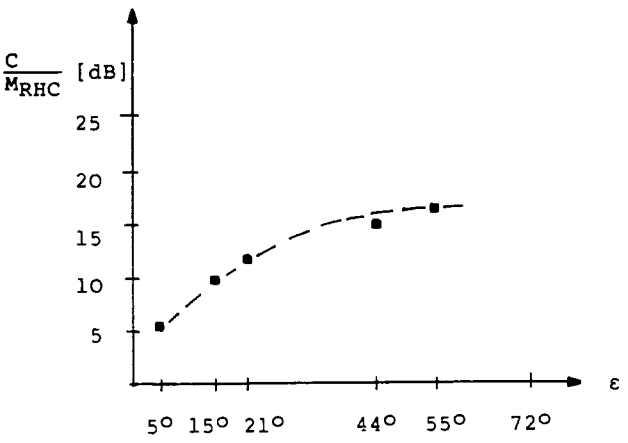

Fig. 3.5: C/M for preoperational 3 dB antenna

To illustrate occuring signal fluctuations, a typical part of the normalized envelope power level P(t) versus time can be seen in Fig. 3.6.

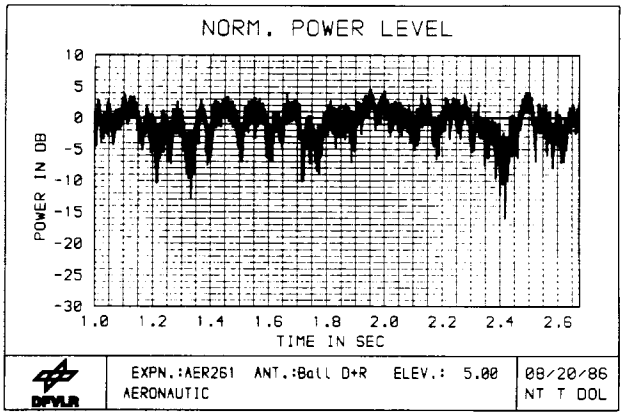

Fig. 3.6: Typical example of a time interval of P(t)

From the stochastic P(t) very useful fading statistics can be derived. A fade is defined as the event that the received power level is below a certain threshold. In the following the thresholds "mean power (0 dB)" and "5 dB below mean power"are considered.

Fig. 3.7 shows the mean fade duration T_{fmean} versus satellite elevation obtained from processing the data of five measurement flights.

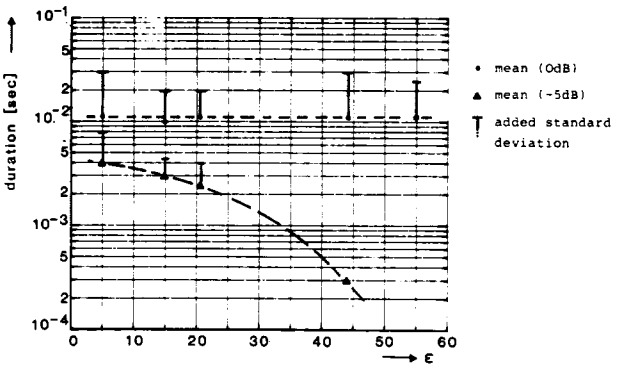

Fig. 3.7: Mean fade duration

The mean fade duration for the 0 dB threshold is almost constant over the elevation angle, for the -5 dB threshold, it decreases significantly. It should be noticed that the standard deviation is relatively high.

Furthermore, the maximum fade duration T_{fmax} and the duration value $T_{f99.9}$ which is with a probability of 99.9% not exceeded by a fade, are of interest. Both values are presented in Fig. 3.8 for the low elevation flights.

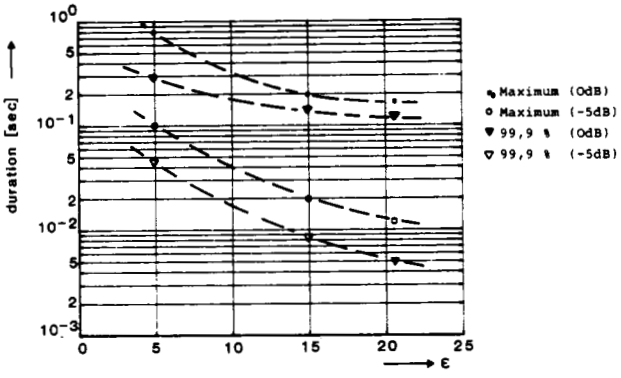

Fig. 3.8: Maximum and 99.9% fade duration

The complementary event to a fade is a connection. Figures 3.9 and 3.10 show the results for T_{cmean}, T_{cmax} and $T_{c99.9}$.

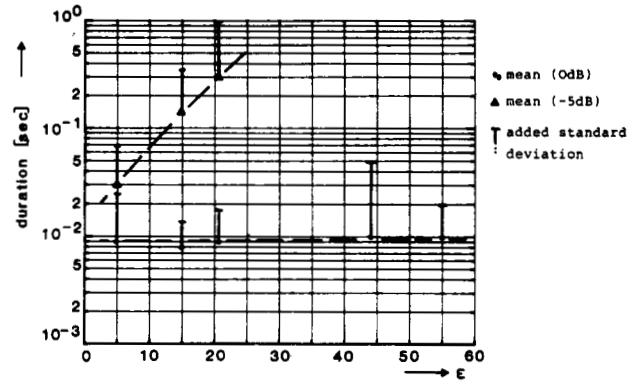

Fig. 3.9: Mean connection duration

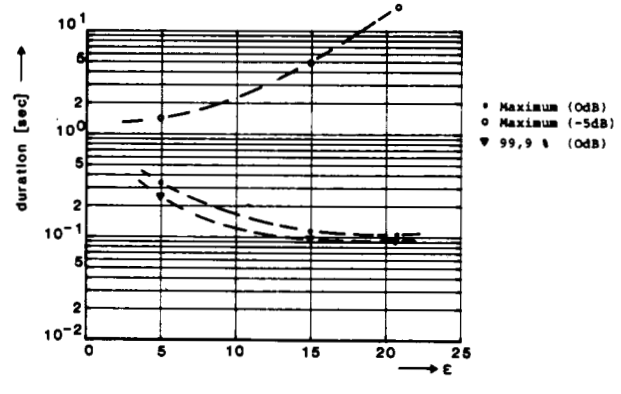

Fig. 3.10: Maximum and 99.9% connection duration

BIT-ERROR RATE MEASUREMENTS

To supplement the knowledge of the aeronautical channel behaviour DECPSK-data transmission experiments had been performed inflight and in the lab, using the stored channel simulator. As a reference, Fig. 4.1 shows the performance of the coherent demodulator with combined COSTAS/AFC-loop [9] for the AWGN channel.

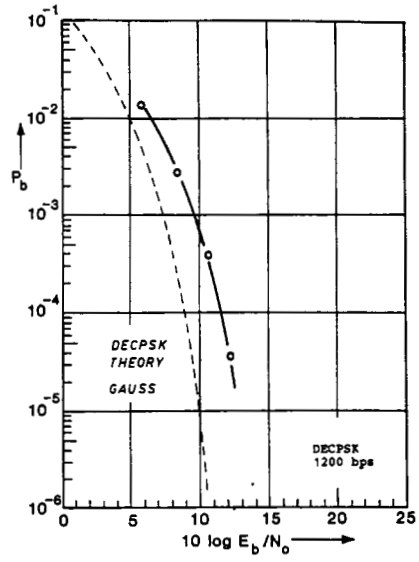

Fig. 4.1: Performance of demodulator in the AWGN channel.

From a variety of measurements figures 4.2 a-c are selected as representative BER-results.

It can be seen that:

- there is a good coincidence between stored channel and inflight measurements
- rate 1/2, constraint length seven convolutional coding combined with interleaving is appropriate to compensate for fading degradation
- BER depends heavily on elevation angle.

It should be noted, that further optimization of recovery loop parameters in the laboratory resulted in general improvements in the order of 2 dB.

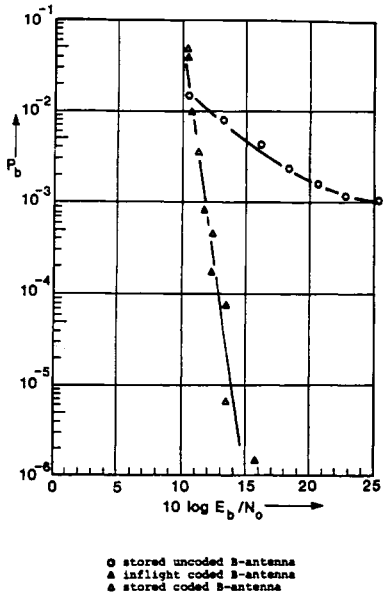

Fig. 4.2a: Bit error rates representing flights over salt-water at 5° elevation angle
C/M = 7.5 dB)

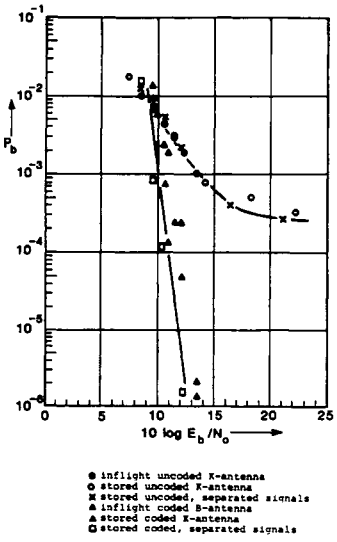

Fig. 4.2b: Bit error rates representing flights over salt water at 15° elevation angle
(C/M = 13 dB)

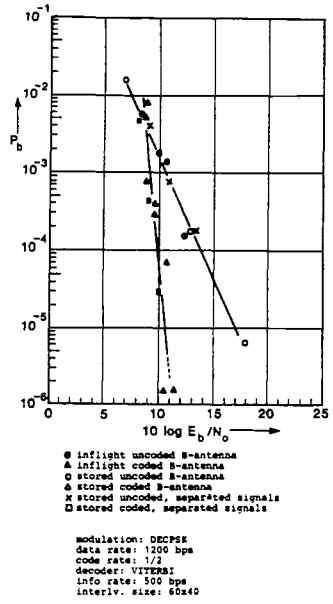

Fig. 4.2c: Bit error rates representing flights over land at 24° elevation angle
(C/M = 15 dB)

CONCLUSIONS

As the channel quality depends heavily on the elevation angle and the antenna of an aircraft, a data transmission system should be designed so that it is able to adapt to widely varying channel conditions. To support such a system design, measurement results characterizing the aeronautical satellite channel at L-band frequencies were presented and partly compared to known theoretical models.

ACKNOWLEDGEMENTS

We would like to thank INMARSAT, for granting permission to use the MARECS satellite, Mr. Exner and Mr. Mahler of the Deutsche Bundespost for obtaining permission from INMARSAT as a signatory, ESA for use of the ground-earth-station Villafranca, our collegues from the institute of high-frequency engineering for providing steerable high gain antennas and the DFVLR flightcrew for implementation of the flying part of the field trials.

LITERATURE

(1) J. Hagenauer, A. Neul, et al., "The Aeronautical Satellite Channel" Draft Final Report, DFVLR, 1986.

(2) P.A. Bello, "Characterization of Randomly Time-Variant Linear Channels", IRE Trans. Comm. System., Vol. CS-11, pp. 360-393, Dec. 1963.

(3) P.A. Bello, "Aeronautical Channel Characterization", IEEE Trans. Comm., Vol. COM-21, pp 548-563, May 1973.

(4) ATS-6, "Air Traffic Control Experimentation and Evaluation with the NASA ATS-6 Satellite", Final Report No. FAA-RD-75-173-V, Febr. 1976.

(5) International Civil Aviation Organization, Special Committee on Future Air Navigation System (FANS)-Report of the 3rd Meeting, Montreal, Nov. 1986.

(6) G. Splitt, H. Forster, "Eine konforme Flugzeug-Array-Antenne mit schwenkbarer Strahlungscharacteristik zur Satellitenkommunikation im L-Band, DFVLR-FB 86-47.

(7) J. Hagenauer, W. Papke, "Data Transmission for Maritime and Land Mobile Using Stored Channel Simulation", Proc. of the 32nd IEEE Vehicular Techn. Conference, San Diego, May 1982, pp. 379-383.

(8) P. Beckmann and A. Spizzichino, "The Scattering of Electormagnetic Waves from Rough Surfaces". New York: Pergamon, 1963.

(9) R. Schweikert, W. Papke, "Performance of a COSTAS/AFC Binary PSK Receiver in a Maritime Satellite Channel", Proc. ICDSC-7, Munich, May 1986.

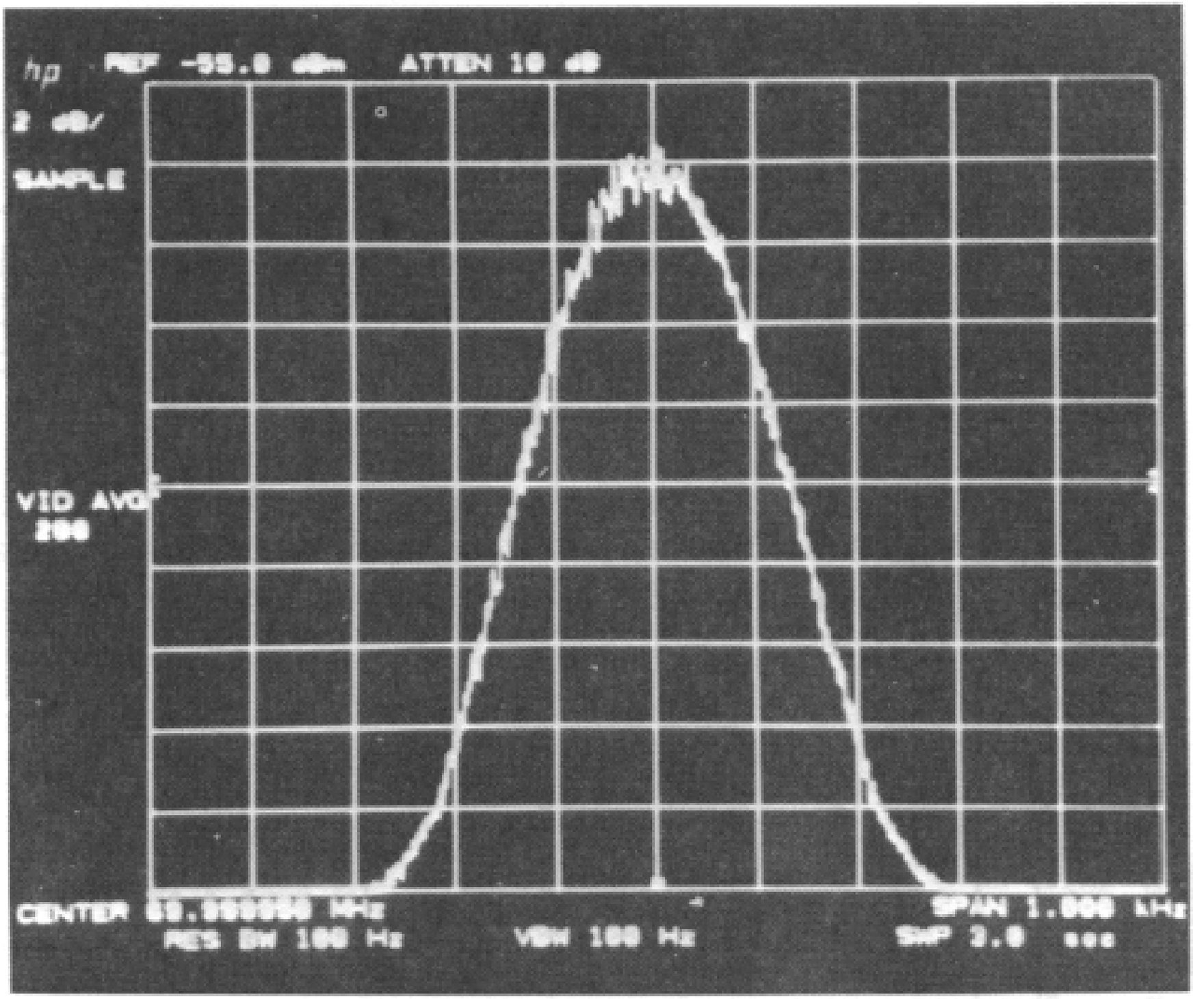

Fig. 3.2: Power-spectrum of RHC reflected signal at $\varepsilon = 15^{o}$ elevation angle